Modeling and Analysis of Proactive and Reactive Defragmentation Approaches in Spectrally-Spatially Elastic Optical Networks

Imran Ahmed†, Bijoy Chand Chatterjee‡, and Eiji Oki†
†Kyoto University, Kyoto, Japan ‡South Asian University, New Delhi, India

***Abstract*—The rapid growth of Internet traffic has intensified the demand for high-capacity and flexible optical networks. Spectrally-spatially elastic optical networks (SS-EONs), leveraging multi-core multi-mode fibers, provide significant capacity enhancement by incorporating spatial dimensions (cores and modes) along with spectral resources. However, these additional dimensions introduce complexity in routing, spectrum, core, and mode allocation and exacerbate spectrum fragmentation, which reduces resource utilization and increases the blocking probability (BP). Defragmentation approaches, classified as proactive and reactive, are essential to mitigate fragmentation without disrupting ongoing traffic. This paper develops exact continuous-time Markov chain (CTMC) models to analyze both proactive and reactive defragmentation approaches in SS-EONs while accounting for inter-core and inter-mode crosstalks. The introduced models incorporate multi-class traffic with varying spectrum demands and utilize a core-mode-spectrum first-fit allocation policy. For large-scale scenarios, an iterative approximation model is also developed. Numerical results demonstrate that proactive defragmentation reduces the probability of waiting requests, making it suitable for delay-sensitive applications, whereas reactive defragmentation achieves lower BP and improves resource utilization. Analytical results closely match Monte Carlo simulations, validating the effectiveness of the proposed models in the performance evaluation of SS-EONs under both defragmentation approaches.**

***Index Terms*—Elastic optical network, defragmentation, blocking analysis, space division multiplexing, Markov chain.**

I. Introduction

The exponential growth of Internet traffic from video-on-demand, cloud computing, and data-intensive applications has strained network capacity. Traditional elastic optical networks (EONs) using single-core fibers cannot meet these escalating demands. Integrating space division multiplexing (SDM) with EONs has led to spectrally-spatially elastic optical networks (SS-EONs) [1], [2], which employ multi-core multi-mode fibers (MCMMFs) to substantially enhance capacity by supporting multiple cores and modes simultaneously [1], [2].

The spatial dimensions of cores and modes significantly complicate resource allocation in SS-EONs, manifesting as the routing, spectrum, core, and mode allocation (RSCMA) problem [2]. Effective RSCMA requires satisfying six constraints: spectrum contiguity (consecutive slot allocation), spectrum continuity, core continuity, mode continuity, and mitigation of inter-core and inter-mode crosstalks (IC-XT and IM-XT) [1], [2]. The continuity constraints ensure that selected spectrum, core, and mode combinations remain consistent along the entire path. IC-XT arises from interference between adjacent cores using identical spectrum slots, while IM-XT occurs when modes within the same core share spectrum slots. Both crosstalk (XT) forms degrade signal quality and network performance.

In dynamic traffic scenarios, spectrum fragmentation poses a persistent challenge. As lightpath requests are established and released over time, isolated gaps in the spectrum accumulate, violating contiguity and continuity constraints [1], [2]. This fragmentation reduces spectrum utilization and increases the blocking probability (BP), where legitimate requests are rejected. In SS-EONs, the fragmentation problem is further complicated by the addition of spatial dimensions. Addressing fragmentation requires either preventive measures during lightpath establishment or adaptive adjustments over time. Defragmentation approaches aim to consolidate gaps created by terminated lightpaths without disrupting ongoing traffic and are broadly classified into reactive and proactive approaches. Reactive defragmentation is triggered by the arrival of a new request, whereas proactive defragmentation operates continuously, independent of incoming requests. Fragmentation intensifies rejection rates, directly impacting BP, a critical metric that quantifies the fraction of rejected requests [3].

Prior studies [4], [5] have examined BP analysis and defragmentation in EONs using continuous-time Markov chain (CTMC) models. However, these models do not capture the additional complexities of SS-EONs, including core and mode dimensions and XT considerations. Recent work [6] proposed an exact CTMC model for reactive defragmentation in SS-EONs, accounting for XT, but did not explore the proactive approach.

Managing fragmentation in SS-EONs is critical, and both proactive and reactive approaches have distinct advantages [3]. Proactive defragmentation reduces the probability of waiting requests, making it suitable for delay-sensitive applications, while reactive defragmentation can achieve lower BP and better resource utilization when some waiting is acceptable [3], [4]. The selection of the appropriate approaches depends on application requirements and operational objectives. To the best of our knowledge, no existing work has modeled and analyzed both proactive and reactive defragmentation approaches in SS-EONs, which is essential for application-centric network design.

This paper addresses this gap by modeling and analyzing proactive and reactive defragmentation in SS-EONs. We develop exact CTMC models that incorporate both approaches while avoiding XT. Our models enable retuning of existing

This work was supported in part by JSPS Postdoctoral Fellowship Program for Research in Japan and JSPS KAKENHI, Japan, under Grant Numbers 25KF0055 and 25K22800.

lightpaths using proactive defragmentation when a lightpath terminates and reactive defragmentation upon the arrival of a new lightpath request, all without disrupting ongoing traffic [7]. The models construct a state transition diagram to consolidate fragmented spectrum slots, allowing estimation of state probabilities. Multi-class traffic requests with varying spectrum requirements are considered, and the core-mode-spectrum first fit (CMS-FF) allocation policy is applied. For large-scale scenarios, we introduce an iterative approximation model for single-hop allocations. Using these models, we evaluate BP and the probability of waiting requests under three scenarios: proactive defragmentation, reactive defragmentation, and no defragmentation. The numerical results show that proactive defragmentation yields a lower probability of waiting requests, while reactive defragmentation achieves lower BP. The analytical results closely match those of Monte Carlo simulations, validating our approach.

II. Resource Allocation with Crosstalk Mitigation and Defragmentation

This section presents a resource allocation approach that manages IC-XT and IM-XT while addressing fragmentation in SS-EONs. XT management typically employs two approaches: XT-avoided and XT-aware [1], [2], [6]. Although XT-avoided offers simpler management, XT-aware provides potentially superior performance at greater complexity. Our analytical models adopt the XT-avoided approach with streamlined policies [6], [8], enabling straightforward transition to XT-aware implementation when required. The approach constructs an auxiliary graph from the MCMMF structure, where adjacency relationships are determined using established XT models and an operator-defined threshold. Two vertices become adjacent when predicted XT exceeds this threshold; otherwise, they remain non-adjacent. The models prohibit identical spectrum assignments across adjacent cores and modes when XT surpasses the threshold, effectively mitigating physical layer impairments. The auxiliary threshold exhibits an inverse relationship with graph connectivity: higher thresholds yield fewer adjacent pairs, relaxing adjacency constraints. As the threshold approaches infinity, the graph becomes disconnected, causing the approach to emulate XT-aware behavior and permit unrestricted spectrum utilization. Our analytical models maintain broad applicability by accommodating alternative XT thresholds or models during auxiliary graph construction, ensuring flexibility across diverse network scenarios.

We show how defragmentation reduces fragmentation while managing IC-XT and IM-XT through an XT-avoided approach in SS-EONs, as illustrated in Fig. 1. Defragmentation rearranges existing lightpaths to mitigate fragmentation without disrupting traffic [7]. We consider a 2-core fiber (p_1, p_2), where each core supports two modes (q_1, q_2) with six spectrum slots per mode, as shown in Fig. 1(a). To prevent XTs, cores and modes are organized into vertices, and XT between each pair of vertices is determined by established XT model [1], [6], [8]. Vertex pairs are designated adjacent if their XT exceeds an operator-defined threshold; otherwise, they remain non-adjacent. These adjacency relationships form an auxiliary graph depicted in Fig. 1(b). We examine nine lightpath requests (LRs 1–9) requiring one, one, two, one, one, one, two, two, and three slots, respectively, to satisfy their bandwidth demands.

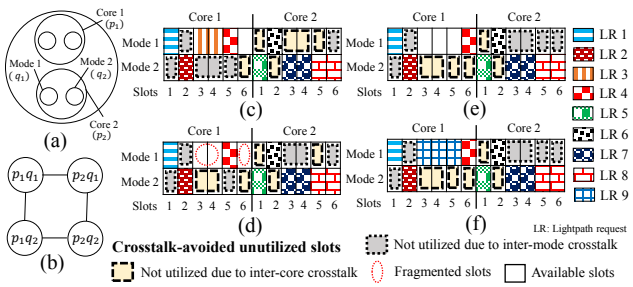

Fig. 1: Demonstration of resource allocation and defragmentation: (a) a structure of 2-core 2-mode fiber, (b) adjacency of cores and modes, (c) initial state of core, mode, and spectrum, (d) LR 3 is terminated and fragmented slots are created, (e) defragmentation is performed using retuning, and (f) state of core, mode, and spectrum after defragmentation and LR 9 is allocated.

Initially, LRs 1–8 are allocated as shown in Fig. 1(c). When LR 3 is released in Fig. 1(d), fragmentation prevents assignment of LR 9, which requires three contiguous slots. Although slots 3, 4, and 6 are available in mode 1 of core 1, they are non-contiguous. Defragmentation shifts LR 4 from slot 5 to slot 6, creating three consecutive slots (3, 4, 5) for LR 9, as illustrated in Figs. 1(e)-(f). SS-EONs impose two critical XT constraints [1], [6], [8]. The IC-XT constraint prohibits identical spectrum slots in the same mode across neighboring cores, while the IM-XT constraint prevents identical slots across adjacent modes within the same core. For instance, in Fig. 1(f), occupying slot 1 in mode 1 of core 1 blocks slot 1 in mode 1 of core 2 (IC-XT) and slot 1 in mode 2 of core 1 (IM-XT). Such blocked slots are termed XT-avoided unutilized slots. However, XT effects become negligible when different spectrum slots are used. Consequently, slot 1 occupancy in mode 1 of core 1 permits slot 2 usage in mode 1 of core 2 (negligible IC-XT) and in mode 2 of core 1 (negligible IM-XT), as demonstrated in Fig. 1(f).

III. Description of Analytical Models

This paper presents analytical models incorporating proactive and reactive defragmentation with XT-mitigating resource allocation under predetermined threshold criteria. Lightpath requests are admitted only when sufficient spectrum resources satisfy three constraints: IC-XT, IM-XT, and spectrum contiguity. Spectrum reorganization is triggered when resources exist but are fragmented across non-contiguous slots. Reactive defragmentation suspends the triggering request until reorganization completes, while proactive defragmentation activates upon request termination without requiring incoming requests to wait. The retuning duration follows an exponential distribution with parameter $1/\mu_d$ [4], proceeding iteratively toward the

initial spectrum slot position when successful establishment is possible post-defragmentation.

The models define two types of state: normal states (no ongoing retuning) and defragmentation states (active retuning). Within defragmentation states, established requests occupying allocated resources are termed active requests, while newly arrived requests awaiting retuning are waiting requests. A transition function $\delta(y,x)$ represents transitions between defragmentation state $y \in X_{\mathrm{D}}$ and normal state $x \in X$ as follows: (i) upon defragmentation completion, the transition rate from state y to $x \in X$ is $\mu_{\mathrm{d}}/|X_y^+|$ if $x \in X_y^+ \cap X$, (ii) when an active request completes service during retuning, a waiting request is immediately accommodated at rate $s_r \times \mu_r/|X_y^{r,-}|$ if $x \in X_y^{r,-} \cap X$, where s_r denotes the number of active class $r \in R$ requests in state y. The condition $\delta(y,x) = 0$ indicates that normal state $x \in X$ is unreachable from defragmentation state $y \in X_{\mathrm{D}}$. Table I presents the notation for symbols used throughout this paper.

TABLE I: Notation and parameter definitions

Given Parameters	
P	Set of available cores in SS-EON
Q	Set of modes per core
W	Set of spectrum slots per mode
R	Set of lightpath request classes based on slots requirements
λ_{pqr}	Arrival rate for class $r \in R$ requests utilizing mode $q \in Q$ of core $p \in P$
μ_{pqr}	Service rate for class $r \in R$ requests utilizing mode $q \in Q$ of core $p \in P$
f_r	The spectrum slot requirements for each request in class $r \in R$
Decision Variables	
X	Complete state space encompassing all possible states
$X_x^{pqr,+}$	Set of reachable states following arrival of a class $r \in R$ request at state $x \in X$ on mode $q \in Q$ of core $p \in P$
$X_x^{pqr,-}$	Set of reachable states following departure of a class $r \in R$ request at state $x \in X$ on mode $q \in Q$ of core $p \in P$
X_{D}	Set of defragmentation states, where $X \cap X_{\mathrm{D}} = \emptyset$
$X_y^+ \subseteq X \cup X_{\mathrm{D}}$	Set of states coming from state $y \in X_{\mathrm{D}}$ after defragmentation for each request
$X_y^{r,-} \subseteq X \cup X_{\mathrm{D}}$	Set of states coming from state $y \in X_{\mathrm{D}}$ when a request in class $r \in R$ completes its service during defragmentation

A. Demonstration of how to create states

To demonstrate state generation, we consider the following parameters: $|P| = 2$, $|Q| = 2$, $|W| = 4$, and $|R| = 2$, where class 1 and class 2 requests require one ($f_1 = 1$) and two ($f_2 = 2$) slots, respectively. The MCMMF comprises two cores, each supporting two modes, as shown in Fig. 1(a). The IC-XT and IM-XT relationships follow the adjacency configuration in Fig. 1(b) based on the XT model from [1], [6], [8]. Each state is represented as $\{(w_1^{1,1}, w_2^{1,1}, w_3^{1,1}, w_4^{1,1}), (w_1^{1,2}, w_2^{1,2}, w_3^{1,2}, w_4^{1,2}), (w_1^{2,1}, w_2^{2,1}, w_3^{2,1}, w_4^{2,1}), (w_1^{2,2}, w_2^{2,2}, w_3^{2,2}, w_4^{2,2})\}$, where $w_i^{p,q}$ denotes slot i occupancy in mode $q \in Q$ of core $p \in P$. Available slots are marked "0", while "1" and "2" indicate slots serving class 1 and class 2 requests, respectively. The notation σ designates XT-avoided slots, α represents slots under retuning, and σ_α identifies XT-avoided unutilized slots during retuning. Normal states x appear in white, while defragmentation states y are shown in brown. Fig. 2 illustrates the state transition diagram for proactive and reactive defragmentation under the CMS-FF policy. The system initializes at state $x = 1$ with all resources available: $\{$(0, 0, 0, 0), (0, 0, 0, 0), (0, 0, 0, 0), (0, 0, 0, 0)$\}$. A class 1 arrival at state 1 allocates slot 1 in mode 1 of core 1, transitioning to state 2 at rate λ_1. IC-XT and IM-XT constraints at state 2 prohibit allocating slot 1 in mode 1 of core 2 and mode 2 of core 1. Service completion returns the system to state 1 at rate μ_1. Through successive arrivals and departures, states $x = 5, 11, 28, 68$, and 157 emerge progressively, ultimately generating $|X| = 841$ total normal states. Fig. 2 presents a representative subset due to space constraints.

Figure 2(a) illustrates proactive defragmentation under the CMS-FF policy. When a class 1 request terminates at normal state $x = 68$ (one of $|X| = 841$ total states) at rate μ_1, two non-contiguous slots become available. Since an incoming class 2 request requiring two contiguous slots cannot be allocated, proactive defragmentation is triggered, transitioning to defragmentation state $y = 1$ with representation $\{$(1, 2, 2, 1), (σ_α, σ_α, σ_α, σ_α), (σ_α, σ_α, σ_α, σ_α), (α, α, α, 0)$\}$. Upon retuning completion, the system returns to a normal state at rate μ_{d} (red arrow from $y = 1$).

Figure 2(b) illustrates reactive defragmentation under the CMS-FF policy. At normal state $x = 157$, an arriving class 2 request cannot be allocated due to fragmentation, triggering reactive defragmentation and transition to state $y = 2$ with representation $\{$(1, 2, 2, 1), (σ_α, σ_α, σ_α, σ_α), (σ_α, σ_α, σ_α, σ_α), (α, α, α, 0)$\}$. In state $y = 2$, in the absence of additional arriving requests during defragmentation, the system exits state $y = 2$ through two ways: (i) retuning completion returns the system to a normal state at rate μ_{d} (red arrow from $y = 2$), (ii) when an active request completes service during retuning, the waiting request is immediately allocated at rate $3\mu_2$ (where 3 equals the number of active requests), transitioning to a pre-existing state (purple arrow from $y = 2$).

B. Analysis of models

This section presents a detailed explanation and analysis of analytical models. We develop equilibrium equations describing steady-state behavior for normal state $x \in X$ in SS-EONs [4], [6]:

$$\Big(\sum_{p\in P}\sum_{q\in Q}\sum_{r\in R, X_x^{pqr,+}\neq\emptyset}\lambda_{pqr} + \sum_{p\in P}\sum_{q\in Q}\sum_{r\in R, X_x^{pqr,-}\neq\emptyset} j_x\mu_{pqr}\Big)\pi_x = \sum_{z\in X: z\neq x}\Big(\sum_{p\in P}\sum_{q\in Q}\sum_{r\in R: x\in X_z^{pqr,+}}\frac{\lambda_{pqr}}{|X_z^{pqr,+}|} + \sum_{p\in P}\sum_{q\in Q}\sum_{r\in R: x\in X_z^{pqr,-}}\mu_{pqr}\Big)\pi_z + \sum_{y\in X_{\mathrm{D}}}\delta(y,x)\times\phi_y, \forall x \in X. \quad (1)$$

In (1), λ_{pqr} represents the transition rate to state $x \in X$ due to class $r \in R$ requests arrivals using mode $q \in Q$ in core $p \in P$. The factor j_x counts outgoing transitions from state $x \in X$ triggered by departures across all classes in R, while μ_{pqr} quantifies the departure rate from state $x \in X$ when class $r \in R$ requests complete service using mode $q \in Q$ in core $p \in P$. The structure of (1) balances outgoing and incoming probability flows. The left-side quantifies outgoing transitions from state $x \in X$ with probability π_x, comprising: (i) arrivals to state $x \in X_x^{pqr,+}$ (if $X_x^{pqr,+} \neq \emptyset$), and (ii) departures from state $x \in X_x^{pqr,-}$ (if $X_x^{pqr,-} \neq \emptyset$). The right-side quantifies incoming transitions to state $x \in X$ from different states. The right-side

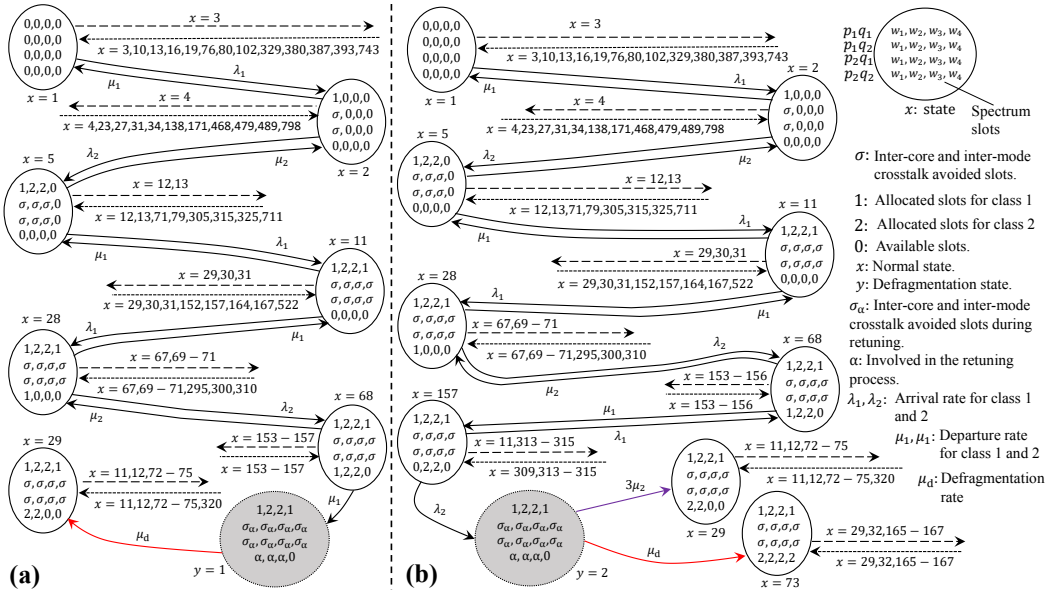

Fig. 2: A segment of state transition diagram under CMS-FF, where $|P|=2, |Q|=2, |W|=4, |R|=2$, $f_1=1$, and $f_2=2$: (a) proactive defragmentation and (b) reactive defragmentation. x indicates a normal state in white color, and y denotes a defragmentation state in brown color. In a state, the label above the rightward arrow indicates the outgoing state from state x, while the label below the leftward arrow indicates the incoming state to state x.

captures three contributions: (i) arrivals from state $z \in X$ to $x \in X_z^{pqr,+}$, (ii) departures from state $z \in X$ to $x \in X_z^{pqr,-}$, and (iii) transitions from defragmentation states to state $x \in X$. For example, applying (1) to state $x=1$ in Fig. 2(a) yields: $(\lambda_1+\lambda_2)\pi_1 = \mu_1(\pi_2+\pi_{10}+\pi_{16}+\pi_{76}+\pi_{102}+\pi_{380}+\pi_{393}+\pi_{743})+\mu_2(\pi_3+\pi_{13}+\pi_{19}+\pi_{80}+\pi_{329}+\pi_{387})$.

Following the model for normal states, the equilibrium equations for defragmentation state $y \in X_{\mathrm{D}}$ are given by [4], [6]:

$$\sum_{p\in P}\sum_{q\in Q}\sum_{r\in R}(s_r\times\mu_{pqr}+\mu_{\mathrm{d}})\phi_y = \sum_{x\in X}\sum_{p\in P}\sum_{q\in Q}\sum_{r\in R:y\in X_x^{pqr,+}}(\lambda_{pqr}+\mu_{pqr})\pi_x + \sum_{g\in X_{\mathrm{D}}\setminus\{x\}}\sum_{p\in P}\sum_{q\in Q}\sum_{r\in R:y\in X_g^{pqr,+}}\lambda_{pqr}\phi_g, \forall y\in X_{\mathrm{D}}. \quad (2)$$

The left-side of (2) quantifies outgoing transitions from state $y \in X_{\mathrm{D}}$ with probability ϕ_y, while the right-side captures incoming transitions from both normal and defragmentation states. For example, applying (2) to state $y=1$ in Fig. 2(a) yields: $\mu_{\mathrm{d}}\phi_1 = \mu_1\pi_{68}$.

The equilibrium equations compute BP and the probability of waiting requests under any spectrum allocation policies. Imposing the normalization constraint $\sum_{x\in X}\pi_x+\sum_{y\in X_{\mathrm{D}}}\phi_y=1$ on (1) and (2) yields a complete system whose solution provides steady-state probabilities π_x for all normal states $x\in X$ and ϕ_y for all defragmentation states $y\in X_{\mathrm{D}}$. The overall BP is computed as $\sum_{x\in B_r}\pi_x+\sum_{y\in B_r^{\mathrm{D}}}\phi_y$, where B_r and B_r^{D} denote the sets of blocking states for normal and defragmentation states, respectively. Similarly, the probability of waiting requests is $\sum_{x\in\chi_r}\pi_x+\sum_{y\in\chi_r^{\mathrm{D}}}\phi_y$, where χ_r and χ_r^{D} represent the sets of waiting states for normal and defragmentation states, respectively.

As the number of cores, modes, and spectrum slots increases, the computational complexity of analytical models also increases. To address this, we employ an iterative approximation model to assess BP under the CMS-FF policy.

Following the approach presented in [6], [8], BP across all traffic classes is approximated as: $\mathrm{BP} = \frac{\sum_{p\in P}\sum_{q\in Q}\sum_{r\in R}\lambda_{pqr}(1-P_1(\Delta,f_r))}{\sum_{p\in P}\sum_{q\in Q}\sum_{r\in R}\lambda_{pqr}}$, where $P_1(\Delta,f_r)$ denotes the probability that at least f_r contiguous available slots can be identified in a pool of Δ total slots. This probability is evaluated as follows: $P_1(\Delta,f_r)=\sum_{i=1}^{f_r-1}\left(P_1(\Delta-i,f_r)(1-\Omega)\Omega^{i-1}\right)+\Omega^{f_r}$, for $f_r\geq 1$. The parameter $\Delta<|X\cup X_{\mathrm{D}}|$ quantifies the total number of states corresponding to available slots, which is determined based on the adjacency relationships between cores and modes, accounting for unutilized slots that mitigate XT effects in SS-EONs. The spectrum utilization factor Ω denotes the bandwidth occupancy ratio. For multi-class traffic scenarios, Ω is formulated as: $\Omega=\frac{1}{\Delta}\sum_{k=1}^{|R|}kP_2(k)$. Here, $P_2(k)$ represents the probability that exactly k slots are currently occupied, which is computed recursively as: $P_2(k)=\sum_{p=1}^{|P|}\sum_{q=1}^{|Q|}\sum_{r=1}^{|R|}f_r(\lambda_{pqr}/\mu_{pqr})P_2(k-f_r)/k$, with boundary conditions $P_2(k)=0$ for $k<0$, and normalization constraint $P_2(0)+\sum_{k=1}^{\Delta}P_2(k)=1$ for $k\geq 1$.

IV. Performance Evaluation

Analytical models are evaluated using BP and the probability of waiting requests, as described in Section III-B. We compare against an analytical model that does not incorporate defragmentation, named Analytical-WODF [8], which enumerates feasible states without defragmentation while satisfying spectrum contiguity, IC-XT, and IM-XT constraints. Our analysis encompasses: (i) Ana-ProDF (proactive defragmentation), (ii) Ana-ReDF (reactive defragmentation), (iii) Analytical-WODF (no defragmentation), (iv) Monte Carlo simulations (Sim-Ana-ProDF, Sim-Ana-ReDF, Sim-

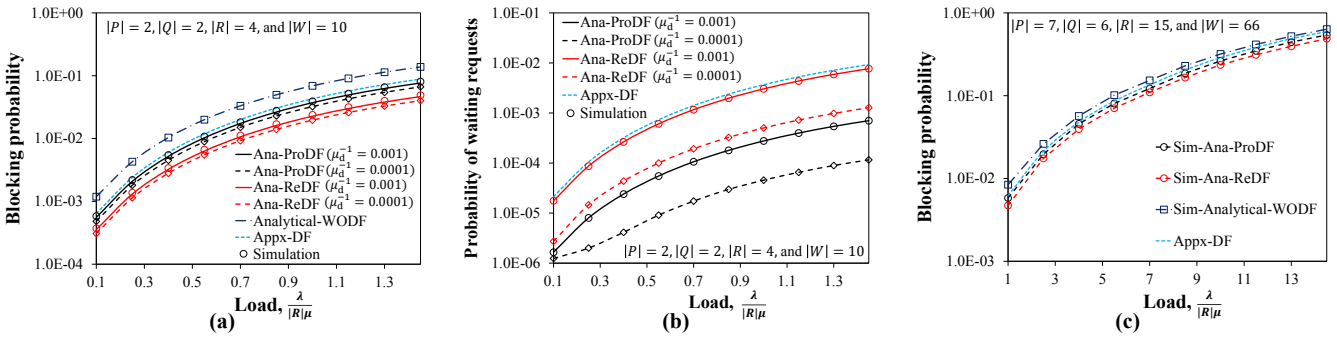

Fig. 3: Comparison of different approaches: (a) BP, (b) probability of waiting requests, and (c) BP for a large-scale scenario.

Analytical-WODF), and (v) Appx-DF (iterative approximation with defragmentation), all under the CMS-FF policy. Experiments run on an AMD EPYC Rome 7502P processor (32 cores, 128 GB memory) with traffic parameters $\lambda_r = (1/|R|)\lambda$ and $\mu_r = \mu$ for all classes $r \in R$. Simulations employ Poisson arrivals (rate λ), exponential service times (mean μ^{-1}), and uniform distribution across $|R|$ classes. All results include 95% confidence intervals with error margins below 5%.

Figure 3(a) compares BP versus load ($\lambda/|R|\mu$) for all approaches with $|P| = 2$, $|Q| = 2$, $|R| = 4$, $|W| = 10$, and defragmentation durations $\mu_{\rm d}^{-1} = 0.001$ and 0.0001 [time unit]. BP increases with load, with Ana-ReDF achieving lower BP than Ana-ProDF for both durations, while Analytical-WODF shows the highest BP. This performance difference stems from the ability of Ana-ReDF and Ana-ProDF to mitigate blocking states through defragmentation approaches, thus reducing overall BP. Ana-ReDF with $\mu_{\rm d}^{-1} = 0.0001$ outperforms $\mu_{\rm d}^{-1} = 0.001$, confirming that longer defragmentation times increase BP. Analytical results closely match simulations, and Appx-DF trends align with Ana-ProDF. Fig. 3(b) presents the probability of waiting request under identical parameters. Ana-ProDF yields lower waiting request probabilities than Ana-ReDF, with Ana-ProDF at $\mu_{\rm d}^{-1} = 0.0001$ outperforming $\mu_{\rm d}^{-1} = 0.001$. Analytical and simulation results show strong agreement, with Appx-DF matching Ana-ReDF. Fig. 3(c) examines large-scale performance ($|P| = 7$, $|Q| = 6$, $|R| = 15$, $|W| = 66$). Sim-Ana-ProDF exhibits a higher BP than Sim-Ana-ReDF, while Sim-Analytical-WODF shows the highest BP. Sim-Ana-ProDF and Appx-DF demonstrate strong alignment across all loads.

V. Direction for Extending Single-Hop Model into Multi-Hop Scenario

Our approach considers multi-hop routes U with Poisson arrivals (rate λ_{pqr}) and exponential service times (mean $1/\mu_{pqr}$) for class $r \in R$ requests using mode $q \in Q$ of core $p \in P$. The average network BP is: $\mathbb{P}_h^{\rm net} = \frac{\sum_{U:h\in U}\sum_{p\in P}\sum_{q\in Q}\sum_{r\in R}(\lambda_{pqr} f_r/\mu_{pqr})\mathbb{P}_r^{\rm res}}{\sum_{U:h\in U}\sum_{p\in P}\sum_{q\in Q}\sum_{r\in R}\lambda_{pqr} f_r/\mu_{pqr}}$, where $\mathbb{P}_r^{\rm res} = 1 - \mathbb{P}_2(\Delta, f_r)$ denotes resource unavailability probability along route U. Resource availability probability is: $\mathbb{P}_2(\Delta, f_r) = \sum_{i=1}^{f_r-1}\left(\mathbb{P}_2(\Delta - i, f_r)(1-\mathbb{P}_U)\mathbb{P}_U{}^{i-1}\right) + (\mathbb{P}_U)^{f_r}$. For spectrum, core, and mode continuity, route-level availability is $\mathbb{P}_U = \prod_{U:h\in U}\mathbb{P}_h$, with individual hop availability $\mathbb{P}_h = 1 - \sum_{U:h\in U}\sum_{p\in P}\sum_{q\in Q}\sum_{r\in R}\lambda_{pqr} f_r/\mu_{pqr}(1-\mathbb{P}_r^{\rm res})/\Delta$, where $\lambda_{pqr} f_r/\mu_{pqr}$ represents offered load and $\lambda_{pqr} f_r/\mu_{pqr}(1-\mathbb{P}_r^{\rm res})$ quantifies carried load. The model is solved iteratively following [6], [8]. Comprehensive BP analysis in multi-hop networks remains a key direction for future research.

VI. Conclusion

This paper modeled and analyzed proactive and reactive defragmentation approaches in SS-EONs while avoiding XT effects. The models enable lightpath retuning upon request termination (proactive) or arrival (reactive) through state transition diagrams that consolidate fragmented slots, allowing state probability estimation. Multi-class traffic with varying spectrum requirements is analyzed under the CMS-FF allocation policy, and an iterative approximation model is developed for large-scale scenarios. The numerical results demonstrate that reactive defragmentation reduces BP by 36-39% compared to proactive defragmentation, while proactive defragmentation reduces waiting probability by 54-90% compared to reactive defragmentation. The analytical results closely match Monte Carlo simulations, validating our approach.

References

[1] B. C. Chatterjee, A. Wadud, I. Ahmed, and E. Oki, "Priority-based inter-core and inter-mode crosstalk-avoided resource allocation for spectrally-spatially elastic optical networks," *IEEE/ACM Trans. Netw.*, vol. 29, no. 4, pp. 1634–1647, 2021.

[2] H. Tode and Y. Hirota, "Routing, spectrum, and core and/or mode assignment on space-division multiplexing optical networks," *IEEE/OSA J. Opt. Commun. Netw.*, vol. 9, no. 1, pp. A99–A113, 2017.

[3] B. C. Chatterjee, S. Ba, and E. Oki, "Fragmentation problems and management approaches in elastic optical networks: a survey," *IEEE Commun. Surveys Tuts.*, vol. 20, no. 1, pp. 183–210, 2017.

[4] S. K. Singh, W. Bziuk, and A. Jukan, "Analytical performance modeling of spectrum defragmentation in elastic optical link networks," *Opt. Switch. Netw.*, vol. 24, pp. 25–38, 2017.

[5] S. K. Singh and A. Jukan, "Computing blocking probabilities in elastic optical networks with spectrum defragmentation," in *Proc. INFOCOM.*, Paris, France, 2019, pp. 424–432.

[6] I. Ahmed, E. Oki, and B. C. Chatterjee, "AnDefrag: Analytical model for blocking probabilities considering defragmentation in spectrally-spatially elastic optical networks," *IEEE Trans. Netw.*, pp. 1–15, 2025.

[7] T. Takagi *et al.*, "Disruption minimized spectrum defragmentation in elastic optical path networks that adopt distance adaptive modulation" in *Proc. ECEOC.*, Geneva, Switzerland, 2011, pp. Mo–2.

[8] I. Ahmed, R. K. Rai, M. Maity, E. Oki, and B. C. Chatterjee, "AnalyticalBP: Analytical model for blocking probabilities considering crosstalk-avoided approach in spectrally-spatially elastic optical networks," *IEEE Trans. Commun.*, vol. 72, no. 3, pp. 1487 – 1501, 2023.